Local orderings in the melting process of a square crystal and in the resulting liquid

E. O. Lima,* P. C. N. Pereira, and S. W. S. Apolinario†
Departamento de Física, Universidade Federal de Pernambuco, 50670-901 Recife, PE, Brazil

(Received 11 July 2022; accepted 12 October 2022; published 3 November 2022)

Using Brownian dynamics simulations we investigate the melting processes of a square crystalline lattice of colloidal particles interacting via an isotropic potential, which comprises both a hard-core repulsion and an additional softened square-well potential. For temperatures slightly lower than the transition one, we found a proliferation of small liquid clusters surrounded by the square lattice. These clusters are not static, quite the opposite, they have an intense dynamics and are continuously formed and destroyed over time. However, no unbound topological defects are observed. At the transition temperature, one of these liquid clusters starts to grow, until the entire system becomes in the liquid phase, then, characterizing a first-order phase transition. The tetratic intermediate phase, as given by the KTHNY theory, was not observed. Moreover, the liquid phase exhibits a considerable number of crystalline clusters having square and triangular orderings, which remain present even when increasing temperature by an order of magnitude. As the temperature increases, structural changes within the liquid phase are analyzed by evaluating the number and sizes of the square and triangular clusters. A transition of the dominant clusters is observed.

DOI: 10.1103/PhysRevE.106.054106

I. INTRODUCTION

The investigation of the melting processes in two-dimensional (2D) systems has been explored for several decades [1–4], and remains a subject of great debate and interest. Much of the efforts to understand melting is aimed at 2D systems whose ordering symmetry is usually triangular. One of the main scenarios concerning melting in 2D systems is given by the Kosterlitz-Thouless-Halperin-Nelson-Young (KTHNY) theory, which states that the melting mechanism of 2D crystals with hexagonal symmetry proceeds via two consecutive continuous transitions: solid-to-hexatic and hexatic-to-liquid transitions [5–7]. The hexatic phase has quasi-long-range orientational order and the analogous case for square crystalline solids is called the tetratic phase.

For a 2D hard-disk system, computer simulations revealed the occurrence of a first-order liquid-hexatic transition and a continuous hexatic-solid transition, which disagrees with the KTHNY theory [8,9]. Many other computer simulation and experimental studies revealed a melting mechanism for 2D solids with contrasting support for a two-stage melting scenario via an hexatic phase as well as a first-order melting transition [10–18]. Based on these results, it seems that 2D melting is not universal, but that depends on the specific properties of the system, e.g., interparticle potential, out-of-plane fluctuations, finite-size effects, etc.

Despite the great effort in understanding the melting processes in 2D crystals with hexagonal symmetry, there are only few investigations addressing the melting of square ordered crystals. Reference [19] found a melting transition of the first order, where a square crystalline lattice, obtained by the combination of two- and three-particle interactions, passes directly to an isotropic liquid. In fact, most square crystals melt this way [20–22], following the prediction of the simplest renormalization group approach of defects-mediated melting in such type of crystals [23].

By adding a higher-gradient term in the theoretical elastic energy of the square lattice, giving a tunable angular stiffness, the first-order transition split into two successive KT transitions [24]. The intermediate tetratic phase has been observed recently, for instance, in systems with isotropic pair interactions [25,26], with hard regular polygons [27] (where many types of solid-to-liquid transitions in 2D appear) and with spinful particles with strong antiferromagnetic interactions [28].

In this work, we investigate the melting processes and the corresponding phases of a 2D system that at zero temperature forms a square crystal. Such type of crystal can appear, for example, in a system with particles interacting through a potential that comprises both a hard-core repulsion and a square-well potential [29,30]. Here we use the softened version of this interaction considered by Ref. [31], which demonstrated, through self-assembly, the formation of a variety of lattice orderings, e.g., triangular, mixed and square orderings, as the well width, α, was varied.

Concerning a 2D square ordered crystal, this paper has the following two objectives: (1) to investigate the solid-liquid transition induced by the temperature increase, and (2) to investigate the characteristics of the resulting liquid phase.

To achieve these goals, we performed a detailed investigation where the different lattice fractions were computed as a function of temperature. It was found that, before the melting, there is a proliferation of liquid clusters throughout the initial squared lattice, where the clusters are continuously formed

*everton.olima@ufpe.br
†sergio.apolinario@ufpe.br

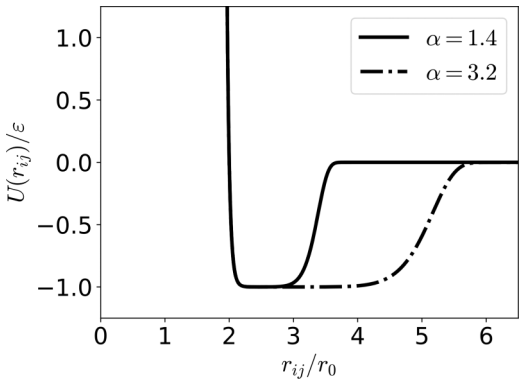

FIG. 1. Representation of the interaction potential, Eq. (1), for two values of the parameter α, with $m = 50$ and $n = 10$.

and destroyed over time. However, at the transition temperature, one of these liquid clusters starts to grow gradually with the increasing of time, until the entire system becomes in the liquid phase, in accordance with the classical nucleation theory [32]. A peculiar characteristic of such a liquid phase is that, although most particles are found in the disordered arrangement, the system also exhibits small clusters with triangular and square orderings. Moreover, the number and sizes of these clusters vary with the temperature and, within the liquid phase, a transition of the dominant type of clusters occurs.

This article is organized as follows: in Sec. II, we present our model, the computational methodology used to control the temperature, and the quantities used to characterize the different orderings of the system. In Sec. III, we present our results and discussions, while the conclusions are given in Sec. IV.

II. THEORETICAL MODEL

A. Details of the simulations

We investigate the melting scenario of a two-dimensional crystalline system of N particles interacting via the isotropic soft square-well potential given by

$$U_{ij} = \varepsilon\left(\frac{2r_0}{r_{ij}}\right)^m - \varepsilon \exp\left[-\left(\frac{r_{ij}/r_0 - 2}{\alpha}\right)^n\right], \qquad (1)$$

where r_{ij} is the distance between the centers of the particles i and j, r_0 defines the radius of the particles, and ε gives the strength of the potential. The smoothness of the left and right edges of the potential well are regulated, respectively, by the exponents m and n, while its width is controled by the parameter α. Figure 1 shows a graphic representation of the interparticle interaction potential [given by Eq. (1)] as a function of r_{ij} for $\alpha = 1.4$ and $\alpha = 3.2$. Throughout the simulations, the following potential parameters were kept constant, that is, $m = 50$, $n = 10$, $r_0 = 1.0$, and $\varepsilon = 1.0$. The total potential energy of the system is given by

$$U = \sum_{i=1}^{N}\sum_{j>i}^{N} U_{ij}. \qquad (2)$$

In previous work [33], it was shown that particles interacting via Eq. (1) can self-organize in at least three different lattice symmetries, that is, square, triangular, and mixed symmetries. Square- and mixed-order lattices appear in two separated ranges, as have been shown by Ref. [33]. The square and mixed orderings occur, respectively, for the intervals $1.03 \leqslant \alpha \leqslant 1.62$ and $3.04 \leqslant \alpha \leqslant 3.32$. In this present work, we take, as an example of the square lattice, the case $\alpha = 1.4$.

For a given temperature, the time evolution system is ruled by the overdamped Langevin equation, which is integrated using the Euler method and, therefore, results in the following first-order algorithm:

$$\vec{r}_i(t + \Delta t) = \vec{r}_i(t) + \frac{\vec{F}_i(t)\Delta t}{\gamma} + \vec{g}_i\sqrt{\frac{2k_BT\,\Delta t}{\gamma}}, \qquad (3)$$

where $\vec{F}_i = -\nabla_{\vec{r}_i}U$ is the total force acting on the particle i, Δt is the finite time step of the integrator, γ is the viscous drag coefficient, k_B is the Boltzmann constant, and $\vec{g}_i$ is a two-dimensional vector with random components, following a standard normal distribution whose mean and variance are equal to zero and one, respectively. Throughout the simulations, both γ and k_B are made equal to one.

All the results will be given in terms of the normalized quantities $r^* = r/r_0$, $U^* = U/\varepsilon$, $T^* = k_BT/\varepsilon$, and $t^* = \varepsilon t/r_0^2\gamma$, respectively, for length, energy, temperature, and time. From now on, for simplicity, we will omit the asterisk in the normalized variables. In other words, lengths are measured in units of r_0, energies in units of ε, temperatures in units of ε/k_B, and times in units of $r_0^2\gamma/\varepsilon$.

To investigate the melting processes the initial configuration is set to be a perfect square crystalline lattice, where the forces acting on any individual particle is null. The algorithm achieves a good convergence for $\Delta t = 10^{-4}$. We iterated the system 2×10^6 time steps before increasing the temperature by an amount of $\Delta T = 0.01$, resulting in a simulation time of $t_{\rm sim} = 200$ for each temperature. We found $t_{\rm sim}$ to be much more than enough for the system to relax at each temperature. At temperature values near the melting, the simulation time that we use is $t_{\rm sim} = 200\,000$.

We considered a system with $N = 256^2 = 65\,536$ particles that interact to each other via the potential of Eq. (1) where $\alpha = 1.4$. In Sec. III A, we consider as the initial configuration the square lattice that minimizes the total potential energy, that is, the one with density $\rho_0 = 0.21473$. In this case, the simulation region is a square box of side $L = 256a_0$, where $a_0 = 2.148291$ is the lattice parameter. In Sec. III B, systems with other density values were investigated. The simulations were carried out with periodic boundary conditions.

B. Order parameters

1. *Standard m-fold orientational order parameter*

In the study of melting, it is useful to calculate some orientational order parameters and their correlation functions. The m-fold bond order parameter of particle j is given by

$$\varphi_m(\vec{r}_j) = \frac{1}{N_j}\sum_{k=1}^{N_j} e^{im\theta_{jk}}, \qquad (4)$$

where N_j is the number of nearest neighbors of particle j, θ_{jk} is the angle formed by an arbitrary reference axis and the distance vectors $\vec{r}_{jk}$. There are different ways to define the neighbors, providing the same qualitative results in our case. In spite of the commonly used Delaunay triangulation, here we use the $N_j = m$ nearest particles as the nearest neighbors, a simple definition which is well-behaved and avoids the discontinuity of the topology of the Voronoi diagram in square crystals (see Fig. 4(b) of Ref. [34]). Thus, for $m = 4$ and $m = 6$, the first four and six nearest particles are used, respectively. The local m-fold bond-orientational order ψ_m is defined as

$$\psi_m = \frac{1}{N}\sum_{j=1}^{N} |\varphi_m(\vec{r}_j)|, \tag{5}$$

while the global m-fold bond-orientational order Ψ_m is defined as

$$\Psi_m = \frac{1}{N}\left|\sum_{j=1}^{N} \varphi_m(\vec{r}_j)\right|. \tag{6}$$

The m-fold bond-orientational correlation function is calculated as

$$g_m(r = |\vec{r}_i - \vec{r}_j|) = \langle \varphi_m^*(\vec{r}_i)\varphi_m(\vec{r}_j)\rangle, \tag{7}$$

where $\langle\rangle$ means an ensemble average. Each phase has a different prediction for the behavior of this correlation function [4,6,27]. In a single crystal, it converges to a nonzero constant at long distances. In the hexatic ($m = 6$) and tetratic ($m = 4$) phases, $g_m(r)$ decays algebraically with the distance, while the isotropic liquid phase presents an exponential decay.

2. *Parameter for symmetry identification*

Colloidal systems with the potential given by Eq. (1) or similar were observed to self-assembly into squared, mixed, and triangular lattices [31,33,35]. For $\alpha = 1.4$ these three lattices have very close energy values so that even a small perturbations can change the local structure. In fact, within the liquid phase of our system, we observed the presence of small crystalline clusters, with square and triangular orders. To further investigate the different local symmetries appearing in our work, we need a method to identify the order around each particle.

Note that any method which is always perfect in the order identification would be complex. For instance, the use of m-BOPs is a relatively simple and generally good method to measure local order, but it has the problem that there can be particles whose local order is visually square-like and whose values of $|\varphi_6(\vec{r}_j)|$ and $|\varphi_4(\vec{r}_j)|$ are the same of some particles which are visually triangular-like. Either way, any good (but not perfect) method would provide the same qualitative informations that we are interested to know in our system. We choose to employ, due to its efficiency, a symmetry parameter ξ_j similar to the one used in Ref. [32]. This single parameter is very simple to calculate and showed to have a good accuracy in identifying clusters' orders in our system. Moreover, it can identify orders that are mixtures of triangular and square ones, which appear in our system.

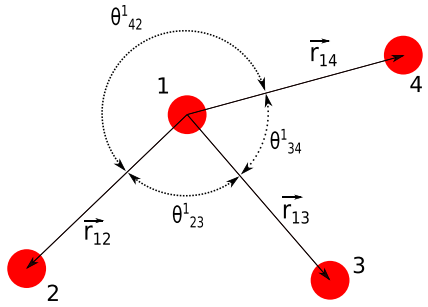

FIG. 2. Schematic representation of a hypothetical configuration formed by four particles which are represented by circles and indexed by numbers from 1 to 4. $\vec{r}_{1k}$ represents the distance vector between particles 1 and k, and θ^1_{kl} represents the smallest angle made by the vectors $\vec{r}_{1k}$ and $\vec{r}_{1l}$, where $k, l = 2, 3$, and 4 with $k \neq l$.

We define

$$\xi_j = \frac{1}{N_j^{\rm cut}}\sum_{\{k,l\}} \sin\theta^{\rm j}_{\rm kl} \tag{8}$$

for a particle j with $N_j^{\rm cut}$ nearest neighbors which are identified through a cutoff radius analysis. The neighbors of j are ordered in the counterclockwise direction and the sum runs over consecutive pairs $\{k, l\}$ of neighbors. θ^j_{kl} is the interbond angle between the neighbor k and the next one l, i.e., the smallest angle formed by the distance vectors $\vec{r}_{jk}$ and $\vec{r}_{jl}$. Note that the angle in Eq. (4) is between a bond and a reference axis, while the angle in Eq. (8) is between two bonds.

Figure 2 shows a schematic representation of a group of four particles, where all the elements needed to calculate the symmetry parameter ξ_j is presented. In this case, the particle 1 has symmetry parameter values equal to $\xi_1 = (\sin\theta^1_{23} + \sin\theta^1_{34} + \sin\theta^1_{42})/3$.

The neighbors' definition used in ξ_j differs from the one used in the calculation of Eq. (4), where a particular type of order (m-fold) is investigated. Here we must be adaptative, since the order around particle j can be square, triangular or other, and we want to identify it. We could use the Voronoi algorithm but it usually gives >4 neighbors for each particle in nonperfect square crystals (see Fig. 4(b) of Ref. [34]). To avoid considering second neighbors as first neighbors, we choose to define the particles k with $|\vec{r}_{jk}| < r_{\rm cut}$ as the neighbors of j. We use the cutoff $r_{\rm cut} = 2.7$, which is around the first valley after the first peak of the radial distribution functions measured in our simulations.

Finally, note that a particle belonging to a perfect triangular lattice has 6 neighboring particles forming angles of $\theta^j_{kl} = \pi/3$ and then $\xi_j \approx 0.866$. For a square lattice, all $\theta^j_{kl} = \pi/2$, so $\xi_j = 1$. In a mixed lattice, as defined in Ref. [31,33] and also called elongated triangular lattice, each particle has three pairs of neighbors with $\theta^j_{kl} = \pi/3$ and two with $\theta^j_{kl} = \pi/2$, and therefore $\xi_j = (3\sin\pi/3 + 2\sin\pi/2)/5 \approx 0.920$. This is the same result obtained in a snub square lattice, as both mixed and snub square lattices are mixtures of square and triangular tillings.

Inspired by the perfect lattices' results and considering small perturbations, we classify particles j having $0.85 \leqslant \xi_j < 0.89$, $0.89 \leqslant \xi_j < 0.94$, and $0.96 < \xi_j \leqslant 1.00$ as being

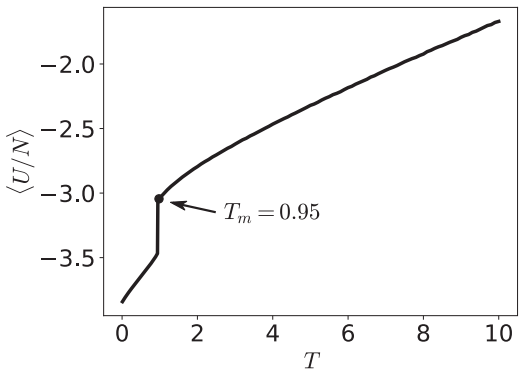

FIG. 3. Time average of the total potential energy per particle, $\langle U/N \rangle$, as a function of temperature, T, for the system with $N = 65\,526 = 256^2$ particles and $\alpha = 1.4$.

triangular, mixed, and square, respectively. The choices of the exact limits of these intervals are not important, they just need to be disjoint, neither too large nor too short, and encompass values around the perfect ones. Note that a "mixed" particle has ambiguity in being of mixed or snub square symmetry, but what matters here is that it has a mixture of triangular and square orders. In fact, in our work, we are interested in the appearance of nonsquare orders within the solid and in the purely square and purely triangular clusters formed within the liquid.

III. RESULTS AND DISCUSSIONS

In this section, we present and discuss the results obtained from overdamped Langevin (Brownian) dynamics simulations used to investigate the colloidal melting processes of the square crystal described in the last section. Crystalline systems, when heated, can change their structural properties and ultimately undergo phase transitions. Considering the square lattice, we intend to answer the following two questions: (1) What phase transitions occur when the system is heated? (2) What characteristics do the phases have near the transition?

In the next subsection we investigate the melting processes of a minimum energy square lattice, that is, a square lattice with $\rho_0 = 0.21473$. Next, in Sec. III B, we consider other density values. The results obtained is summarized in a $T \times \rho$ phase diagram.

A. Minimum energy square lattice: $\rho_0 = 0.21473$

Here we simulate the system with density $\rho_0 = 0.21473$, which is the one that minimizes the total potential energy, Eq. (2), for a square crystal. To determine the phase transition temperature we calculated the time averaged potential energy per particle, $\langle U/N \rangle$, for each temperature T. Figure 3 shows how $\langle U/N \rangle$ varies with T. Such a figure demonstrates that $\langle U/N \rangle$ exhibits, initially, a monotonous increase with the growth of temperature, and that it passes through an abrupt variation between at 0.95. The discontinuity in the potential energy signalizes to the occurrence of a first-order phase transition.

At any $T \leqslant 0.94$, we can see from configuration snapshots that the orientation of the square order is very nearly vertical/horizontal along the whole system, indicating a long range orientational order and thus a crystalline phase. For $T \geqslant 0.95$, we can see from snapshots that there is great disorder and no preferred orientation in the system, indicating an isotropic liquid phase. Some quantitative analysis of the orientational order parameters introduced in Sec. II B 1 are shown in Sec. III A 1. The long and short range orientational orders before and after the transition, respectively, are measured.

As we observe through configuration snapshots before the transition, an isolated dislocation is extremely rare to appear and, when it does, it is still near to a dislocation with opposite Burgers vector. The absence of free dislocations is another indication that this phase is crystalline and not tetratic. Figures with snapshots and discussions about the appearance of disorder near and during the melting are given in Sec. III A 2. Within the liquid, after melting, small clusters with square and triangular orderings are observed. Snapshots, measures and discussions about the crystalline clusters appearing in the liquid phase are given in Sec. III A 3.

1. Orientational order parameter analysis

Here we investigate some aspects of the orientational order in our system by measuring what was defined in Sec. II B 1. Figures 4(a) and 4(b) present, respectively, graphs of the local and global m-fold order parameters, that is, ψ_m and Ψ_m, for $m = 4$ and 6 as a function of the temperature, T. Figure 4(c) shows the fourfold orientational correlation functions, $g_4(r)$, as a function of the radial distance, r, for the temperatures $T = 0.5,\ 0.7,\ 0.94,\ 0.95,\ 1$, and 5.

Before the transition (i.e., $T < 0.95$), Figures 4(a) and 4(b) reveal that the system holds large values of the local and global fourfold bond-orientational parameters (i.e., $\psi_4 \geqslant 0.936$ and $\Psi_4 \geqslant 0.924$, respectively), indicating a square ordered phase. Also, within this range, the correlation function $g_4(r)$ converges, for large values of r, to some constant close to the unity, as shown in Fig. 4(c). This long range orientational order indicates that, before the transition, the system keeps in a square crystal phase.

We can see that the system loses its global orientational order for $T \geqslant 0.95$, becoming an isotropic liquid. However, note that it still maintains some local square order ($0.514 > \psi_4 > 0.405$) and gains a relevant local triangular order which, for $T \geqslant 1.1$, becomes higher than the square one. As it can be seen from configuration snapshots, which will be shown and discussed in Sec. III A 3, the triangular and square orders appear in clusters within the liquid. One could expect that the correlation of the orientational order parameter is high within the length scale of the clusters' sizes and then decays exponentially at large distances. However, as it is shown in Figs. 4(c) and 4(d), both the fourfold and sixfold orientational correlation functions [given by Eq. (7)] decay exponentially even at short distances. The liquid has a purely short range orientational order.

We did not find evidence for the two-stage melting processes described by the KTHNY theory or an adaptation of it for square crystals. Indeed, our simulations demonstrate that the system does not present a regime where $g_4(r)$ [or $g_6(r)$] has an algebraic decay, characteristic of the quasi-long-range orientational order of the tetratic (or hexatic) phase.

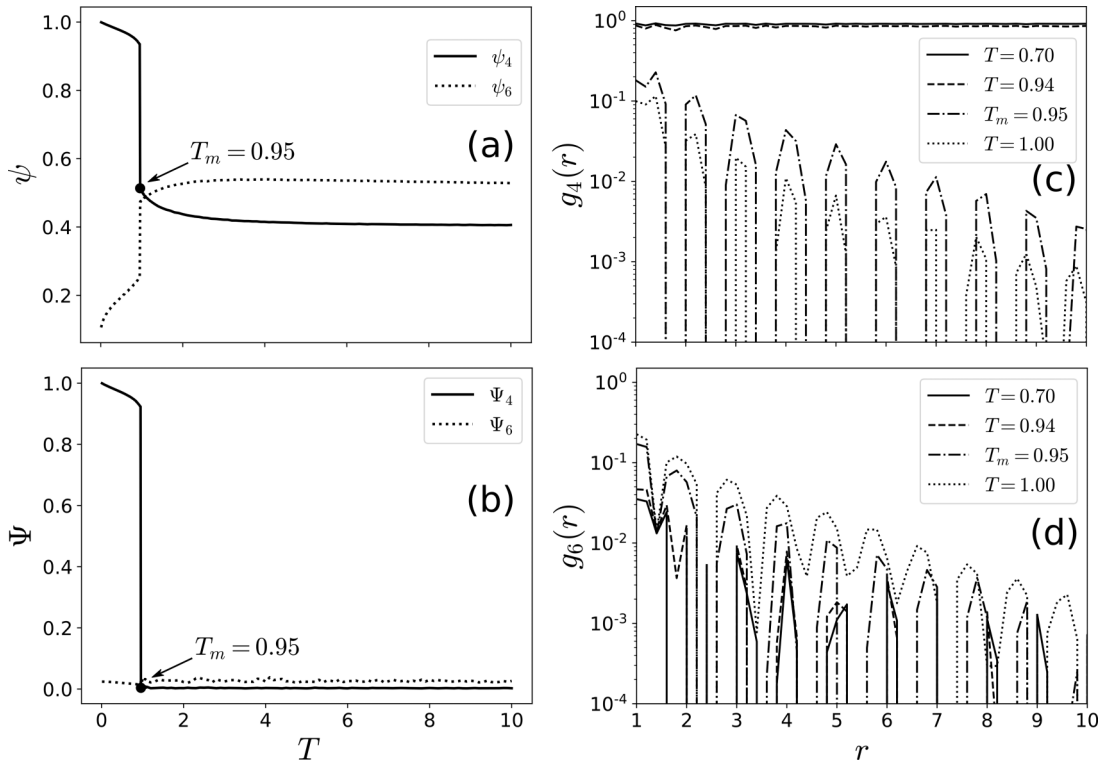

FIG. 4. (a) The local m-fold bond-orientational order parameter, ψ_m, for $m = 4$ (solid line) and $m = 6$ (dotted line) given by Eq. (5), (b) the global m-fold bond-orientational order parameter, Ψ_m, for $m = 4$ (solid line) and $m = 6$ (dotted line) given by Eq. (6), and (c) fourfold and (d) sixfold bond-orientational correlation functions, $g_4(r)$ and $g_6(r)$, for the values of temperature $T = 0.7,\ 0.94,\ 0.95$, and 1, given by Eq. (7).

2. Local symmetry analysis near and during the melting

Particles in the crystalline lattice experience a strong and regular confinement due to the interaction potential created by the neighboring particles. The increasing of the temperature enhances the particles' random motion that eventually allows small regions of the system to change their local order. We observe that, in our system, these changes of order are strongly pronounced, looking like spatially localized phase transitions. This occurs before and after the transition.

At the temperature $T = 0.94$, Figs. 5(a) and 5(b) display distinct snapshots, respectively, for the time values $t = 157\,200$ and $t = 157\,380$. The colored circles in blue, green, and red, represent, respectively, particles with the squared, mixed and triangular orderings. Such a classification for a given particle j was determined by computing the quantity ξ_j and adopting the criteria given in the end of Sec. II B 2. Note that the neighbors of the green particles, assigned with a mixed ordering, seems to be in a mix of square and triangular orderings, but have not necessarily the same symmetry of the mixed lattice of Refs. [31,33].

Figures 5(a) and 5(b) show that the particles belonging to the square symmetry (blue circles) are predominant. Our simulations reveal that particles with the triangular and mixed orderings tend to appear in groups, forming small clusters of disorder within the square order phase, with no net Burgers vector. In other words, the defected regions appearing in the crystal are predominantly local and nontopological. This can be visualized in Figs. 5(c) and 5(d), which are, respectively, enlarged figures of the black square contours displayed in Figs. 5(a) and 5(b). In fact, we observed that a region with nonzero net Burgers vector, representing a dislocation, is extremely rare to appear and, when it does, it is still near to a region with opposite Burgers vector. Such absence of unbound topological defects, before melting starts, maintains the translational order expected in a crystal.

We emphasize that the black squares in Figs. 5(a) and 5(b) are located in the same place of the simulation box but at different times. Therefore, as we can see, the clusters of non-square order in the solid phase are not static and can undergo changes over time. Some defected regions, after appearing, may increase a little but they all disappear after some time, reorganizing back to the square ordering. Indeed, we observed that close particles stay close along the time, i.e., with no relative diffusion, which is another aspect of a solid phase as stated by the dynamic Lindemann criterion [36].

Besides the discontinuities in Figs. 3 and 4(a), 4(b) another indication that we have a first-order phase transition is that the evolution of the melting process is in accordance with classical nucleation theory [32] and has the following characteristics. At $T = 0.95$, a small liquid nucleus is formed and then gradually grows in size as the time passes. This can be verified in Fig. 6, which shows the melting evolution in a simulation of our system after the temperature achieves $T = 0.95$. In Fig. 6(a), which occurs at the time $t = 156400$, a small cluster in the liquid phase is formed. This cluster grows gradually over time, as we can see from Figs. 6(b), 6(c), and 6(d), respectively, for $t = 158\,500$, $t = 160\,500$, and $t = 160\,900$. In this latter, the liquid phase is percolated and occupies almost the entire simulation box, with the exception of a small region with squared symmetry. Ultimately, for even

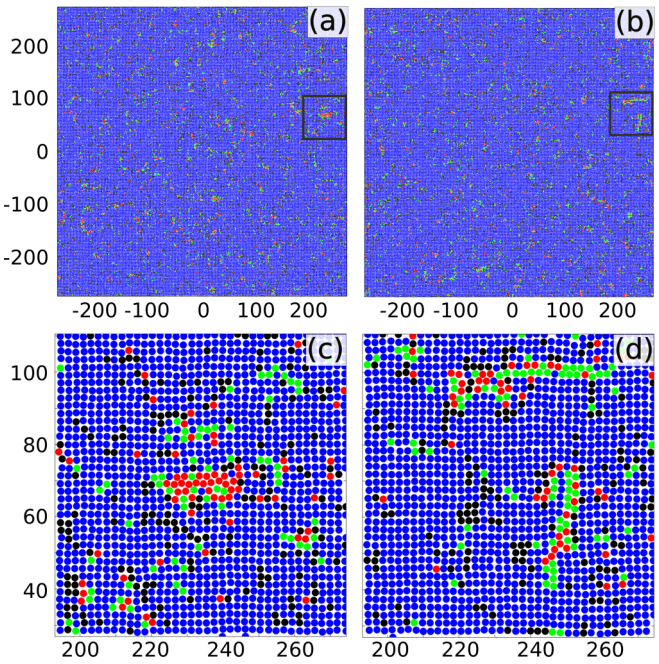

FIG. 5. Panels (a) and (b) show the system configurations at $T = 0.94$, taken at different times along the running simulation. Panels (c) and (d) present, in detail, particles within the squared boundaries, respectively, of panels (a) and (b). To identify the particle's ordering classification, we adopted the criteria presented in the end of Sec. II B 2, where the quantity ξ_j was computed. The colored circles in blue, green, and red indicate, respectively, the presence of particles with square, mixed and triangular orderings. Black filled circles represent particles whose ξ values do not fit into any of these three orderings.

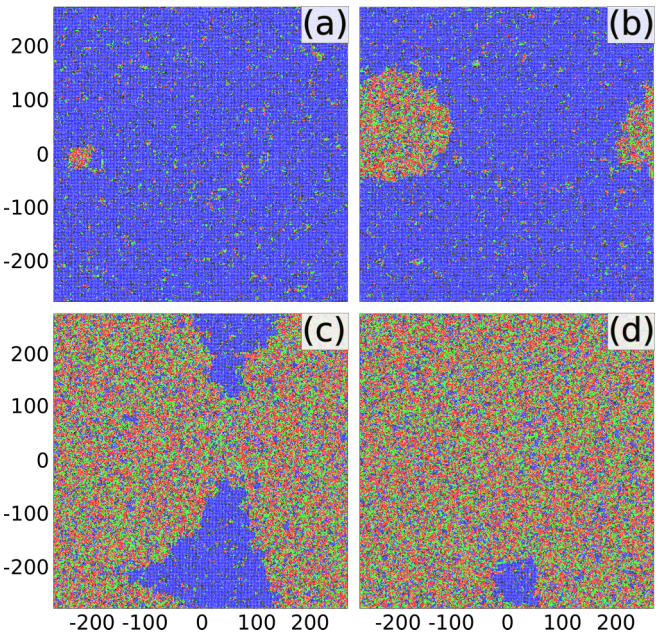

FIG. 6. Configurational snapshots at different times presenting the evolution of the melting for a system at the temperature $T = 0.95$ and whose initial configuration forms a square crystal. The region occupied by the liquid phase gradually grows as time passes. In sequence, from the shortest time to the longest one, we have the snapshots (a), (b), (c), and (d), occurring, respectively, at the times $t = 156\,400$, $158\,500$, $160\,500$, and $160\,900$. The circles are colored as in Fig. 5.

greater growth in time, the liquid phase passes to fill the entire simulation box. We recall that, for temperatures below $T = 0.95$, small "liquid" clusters can be formed, however they are structures with limited lifetime, that is, such local disorders eventually disappear.

3. Local symmetry analysis in the liquid phase

In general, physical systems whose crystalline order is triangular can present, after melting, a disordered structure typical of the liquid phase with occasional triangular clusters [38]. We have already addressed the melting transition process for a square ordering system, but we have not yet talked about how the system behaves after melting, and in particular, if there is any kind of remaining ordering.

The thermodynamic equilibrium phase in our system at the temperature $T = 0.95$ corresponds to a liquid, with diffusion. Figure 7(a) shows a snapshot of a thermodynamic equilibrium configuration at this temperature. As we can see, the system has not a globally preferred order or orientation in contrast to what is found for the system with $T = 0.94$ [see Fig. 5(a)], where the disorder becomes concentrated in small clusters surrounded by a squared lattice.

Figure 7(b) shows in more detail the particles' positions located inside the black square contour of Fig. 7(a). Visually, the local order around each particle within this liquid is rarely noncrystalline. We can see regions with many types of crystalline orderings, varying from square (as blue circles) and triangular (as red circles) to mixed and snub-square (both as green circles). Note, however, that only square and triangular particles form single crystal clusters with considerable size. Due to the dynamical aspect of the liquid, these orderings are constantly changing with the passage of time.

Figure 8(a) shows the number of clusters with triangular and square orderings as a function of the temperature, T. To construct this graph, the procedure we considered to perform the separation of clusters is given in the following. First, we classify all particles according to their value of ξ_i, as described in the end of Sec. II B 2, and then we group neighboring

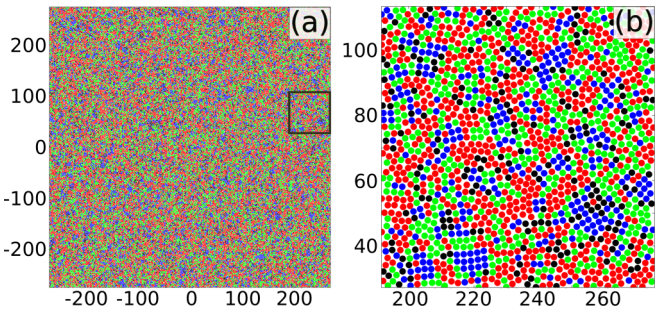

FIG. 7. Panel (a) shows a snapshot for the system in thermodynamic equilibrium at a temperature of $T = 0.95$. Panel (b) shows the particle configuration of the region inside the black square contour in panel (a). The circles are colored as in Fig. 5.

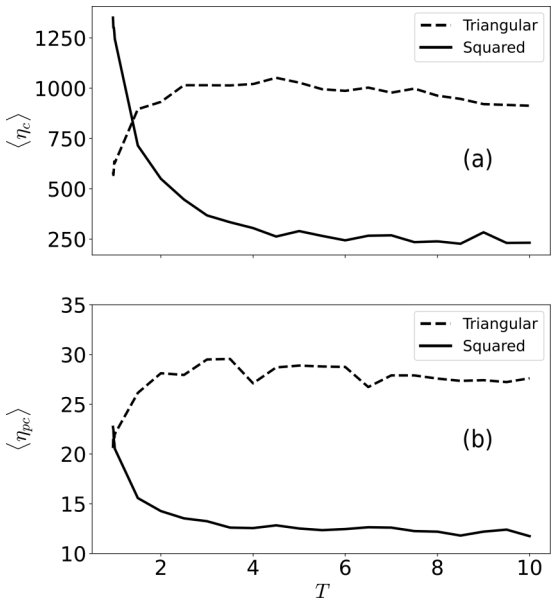

FIG. 8. (a) Average number of clusters, $\langle \eta_c \rangle$, with squared (square dots) and triangular (triangular dots) orderings as a function of the temperature, T. (b) Average number of particles, $\langle \eta_{pc} \rangle$, in clusters with square (square dots) and triangular (triangular dots) symmetries as a function of the temperature, T.

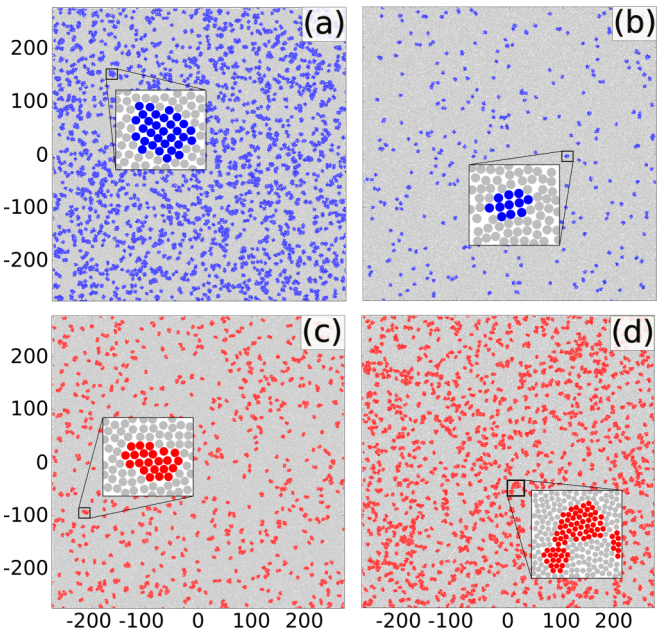

FIG. 9. Configurational snapshots for systems at the thermodynamic equilibrium, where clusters with triangular and square orderings are presented separately. Panels (a) and (c) correspond to a system at $T = 0.95$ while panels (b) and (d) to a system at $T = 5$. The first and second lines display, respectively, only the clusters with square (blue circles) and triangular (red circles) orderings. Zooms are shown to better visualize some clusters.

particles (i.e., particles separated by a distance $< r_{cut} = 2.7$) that have the same local order. Thus, we obtain groups formed by two or more particles with same order where each one is neighbor to at least 1 other particle of the group. A cluster is composed by the particles of a group like this and all their neighbors. Note that the smallest possible square and triangular clusters have 8 and 10 particles, respectively, as they comprise a group of two neighboring particles with same order and their neighbors.

Just after the transition, at $T = 0.95$, the average number of clusters with triangular and square orderings are approximately 583 and 1351, respectively. As the temperature increases, a significant variation in the number of clusters happens, which can be seem from Fig. 8(a). The temperature increase leads, ultimately, to the predominance of clusters having a triangular ordering. This latter fact is in agreement with the behavior observed, previously, by analyzing the bond orientational parameters [see Fig. 4(a)].

For $T = 10.00$, Fig. 8(a) shows that the average number of clusters with triangular and square orderings are approximately 900 and 250, respectively. This shows that the number of clusters with triangular ordering becomes almost four times greater than that of the square ordering. Nevertheless, we have to point out something peculiar for the present system: the number of clusters with square ordering, even at high temperatures, still remains significant. Therefore, the liquid phase of the system is composed by both triangular and square ordered clusters. Such a kind of liquid, presenting clusters with two distinct local crystalline orderings, as far as we know, has not yet been described in the literature.

The increase in temperature not only affects the number of clusters in the system, but also their size. Figure 8(b) presents the average number of particles per cluster, $\langle \eta_{pc} \rangle$, as a function of temperature, for clusters with triangular (see triangular dots) and square (see square dots) orderings. Shortly after the transition, i.e., for $T = 1.0$, we see that the two types of clusters have approximately the same average number of particles, $\langle \eta_{pc} \rangle = 26$. However, as we can see in Fig. 8(b), the increase in temperature leads to the increase of the average number of particles in clusters with triangular order and, oppositely, to the reduction in those with square order. For large values of temperature, $\langle \eta_{pc} \rangle$, approximates to values around 27 and 13, respectively, for clusters with triangular and square orderings.

The change of dominant order of the clusters with increasing temperature is due to the decrease of relative relevance of the interaction potential well. The power-law repulsive part of the potential in Eq. (1), when considered alone at fixed density, induces a triangular ordering [37]. When the attractive part is added, with $\alpha = 1.4$, a certain amount of nearby particles tend to be trapped in the potential well, inducing a square ordering [31]. Right after melting, the potential well is still relevant and many square clusters appear. As the temperature increases, the well depth becomes small when compared to the kinetic energy. In this case, neighboring particles no longer get stuck in the well and their ordering is induced by the power-law repulsion, preferring to form triangular clusters.

To better visualize the clusters with triangular and square symmetries, we present them separately, as follows: Figs. 9(a) and 9(c), referring to the same system at $T = 0.95$, show, respectively, a snapshot containing the configurations with square (blue circles) and triangular (red circles) clusters.

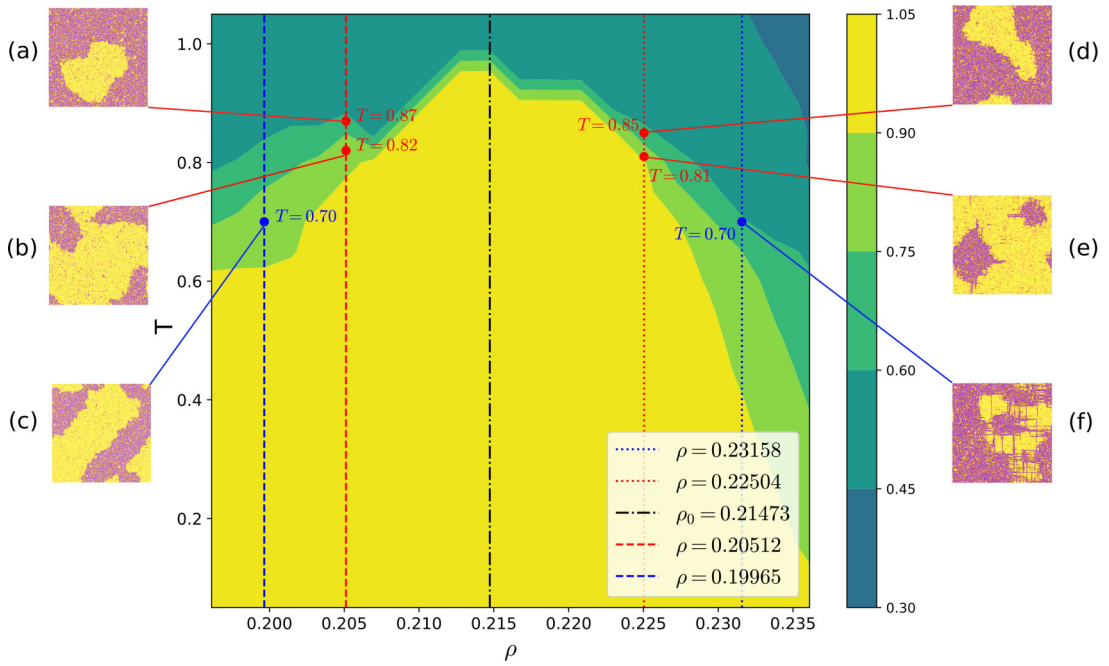

FIG. 10. $T \times \rho$ phase diagram. Colors are based on the ψ_4 values computed for the system. Some snapshots of the system are presented on the sides of the diagram. The vertical lines indicate, from left to right, the following density values: $\rho = 0.19965$, 0.20512, 0.21473, 0.22504, and 0.23158. The case $\rho_0 = 0.21473$ (dashed black line) corresponds to the density for which the square lattice has its lowest energy. For densities inside the interval $0.20512 < \rho < 0.22504$, the system melts directly from a square crystalline solid to a liquid, as described in Sec. III A. For $\rho \leqslant 0.20512$ and $\rho \geqslant 0.22504$, a coexistence of the solid and liquid phases happens.

Similarly, Figs. 9(b) and 9(d), which correspond to a system at higher temperature, that is, $T = 5.0$, present snapshots of the same configuration showing, respectively, the square (blue circles) and triangular (red circles) clusters. These snapshots once more demonstrate that triangular clusters become dominant at high temperatures, although the square order remains present and significant.

B. Other square lattice densities: $\rho \neq \rho_0$

It is pertinent to consider densities with values around ρ_0, since in any real physical situation, the density value carries an experimental error. Figure 10 presents the phase diagram $T \times \rho$ where the values of the local fourfold bond-orientational order parameter ψ_4, computed from the system configurations, are used to give the point colors. We considered the intervals: $0.19613 \leqslant \rho \leqslant 0.23611$ and $0.05 \leqslant T \leqslant 1.05$. The color range varies from yellow ($0.90 < \psi_4 < 1.00$) to dark green ($0.30 < \psi_4 < 0.45$). Some snapshots are displayed for the densities values $\rho = 0.19965$, 0.20512, 0.22504, and 0.23158 (see the vertical lines used to highlight the density locations), and temperatures indicated in figure. The dashed vertical black line in Fig. 10 signalizes the region with the density $\rho_0 = 0.21473$ of the square crystal with minimum potential energy.

The interval $0.20512 < \rho < 0.22504$ corresponds to the central region of the diagram (see Fig. 10), which is delimited by the vertical dashed and dotted red lines. For a density value within this interval, we found that the system melts directly from a square crystalline solid to an isotropic liquid. Thus, reproducing the same scenarios previously found for the system with $\rho_0 = 0.21473$.

Figures 11(a) and 11(b) present the $g_4(r)$ correlation function as a function of the distance r, respectively, for the systems with the density values $\rho = 0.20699$ and 0.22292. These densities are located inside the central interval delimited by the dashed and dotted vertical red lines of the phase diagram of Fig. 10. Figure 11 shows that the systems with density values $\rho = 0.20699$ and 0.22292 melt, respectively, at the temperatures $T_m = 0.85$ and 0.89. From Figs. 11(a) and 11(b), we can see that $g_4(r)$ is converges to a constant, for $T < T_m$, and decays linearly, for $T \geqslant T_m$. Thus, we did not observe the occurrence of the tetratic phase, or even of the hexatic phase. In fact, we calculated $g_4(r)$ and $g_6(r)$ for several points of the phase diagram show in Fig. 10 and no algebraic decay was observed, where the plots of $g_6(r)$ are all similar to the ones shown in Fig. 4(d).

For $\rho \geqslant 0.22504$, the solid and liquid phases can occur simultaneously for the system in thermodynamic equilibrium. This coexistence is common in NVT simulations with first-order transition of phases with different preferred densities. As the size of simulation box is kept constant, there are temperatures at which part of the system must remain in the solid state for the liquid phase to occur. Figures 10(d)–10(f) present configurational snapshots containing the coexistence of phases.

Similarly, phase coexistence also occurs for $\rho \leqslant 0.20512$. Figures 10(a)–10(c) illustrate this situation. Here, the liquid phase is favored due to the decreasing in density, and consequently in pressure, causing part of the system to melt while

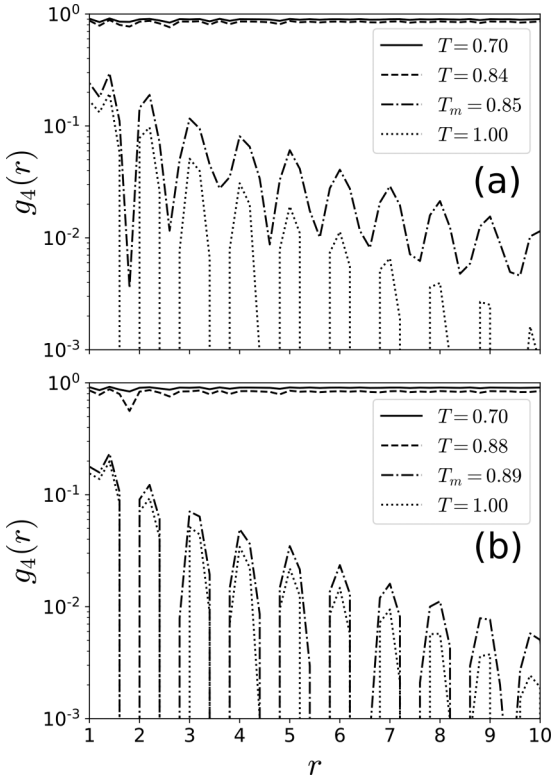

FIG. 11. The orientational correlation function, $g_4(r)$, for the system with $N = 256^2 = 65536$ colloidal particles and densities: (a) $\rho = 0.20699$ and (b) $\rho = 0.22292$. These densities are inside the region delimited by vertical red lines in Fig. 10. T_m is the transition temperature. $g_4(r)$ has a constant behavior for $T < T_m$, and an exponential decay for $T \geqslant T_m$.

another remains solid. Reference [31] considered a similar system with $\rho < \rho_0$, but there, the main focus was on the investigation of self-assembly processes and configurations at zero temperature.

IV. CONCLUSIONS

In this work, we investigated through NVT brownian dynamics simulations the melting process of a 2D system which at zero temperature forms a square lattice. We considered an interaction potential that comprises both a hard-core repulsion and an additional softened square-well potential.

For the square lattice, the density that minimizes the total potential energy is $\rho_0 = 0.21473$. Our simulations demonstrated that the investigated square lattice, having density ρ_0, or a value around it, melts without the intermediation of a tetratic phase analogous to the hexatic one given by the KTHNY theory. Bond-orientational order parameters are used, for instance, to demonstrate such nonoccurrence of this type of intermediate phase. The system thus goes directly from crystal to liquid. Coexistence is observed at high or low densities, as we show in a phase diagram.

We performed a detailed investigation where the different fractions of local orderings were computed as a function of temperature. It was found that, before the melting, there is a proliferation of nonsquare regions throughout the initial squared lattice, which are continuously formed and destroyed over time. In spite of these disordered regions, no unbound topological defects are observed. At the transition temperature, one of these liquid clusters starts to grow with the increasing of time, until the entire system becomes in the liquid phase. This latter constitutes a one step solid-to-liquid first-order phase transition.

A peculiar characteristic of the revealed liquid state is the persistent presence of two distinct types of crystalline clusters, that is, clusters with triangular and square orderings. We located and measured the sizes of these clusters and observed that they are continuously formed and destroyed along the time. These clusters can be relatively big, though the orientational correlation function decays exponentially even at short distances. Transitions between the dominant order of the clusters show the rich variety of structural sub-phases that can be present within the liquid phase.

[1] K. J. Strandburg, Rev. Mod. Phys. **60**, 161 (1988).
[2] J. G. Dash, Rev. Mod. Phys. **71**, 1737 (1999).
[3] U. Gasser, J. Phys.: Condens. Matter **21**, 203101 (2009).
[4] V. N. Ryzhov, E. E. Tareyev, Y. D. Fomin, and E. N. Tsiok, Phys. Usp. **60**, 857 (2017).
[5] J. M. Kosterlitz and D. J. Thouless, J. Phys. C: Solid State Phys. **6**, 1181 (1973).
[6] D. R. Nelson and B. I. Halperin, Phys. Rev. B **19**, 2457 (1979).
[7] A. P. Young, Phys. Rev. B **19**, 1855 (1979).
[8] E. P. Bernard and W. Krauth, Phys. Rev. Lett. **107**, 155704 (2011).
[9] M. Engel, J. A. Anderson, S. C. Glotzer, M. Isobe, E. P. Bernard, and W. Krauth, Phys. Rev. E **87**, 042134 (2013).
[10] K. Zahn, R. Lenke, and G. Maret, Phys. Rev. Lett. **82**, 2721 (1999).
[11] P. Karnchanaphanurach, B. Lin, and S. A. Rice, Phys. Rev. E **61**, 4036 (2000).
[12] Y. Peng, Z. Wang, A. M. Alsayed, A. G. Yodh, and Y. Han, Phys. Rev. Lett. **104**, 205703 (2010).
[13] Y. Han, N. Y. Ha, A. M. Alsayed, and A. G. Yodh, Phys. Rev. E **77**, 041406 (2008).
[14] S. A. Rice, Chem. Phys. Lett. **479**, 1 (2009).
[15] C. A. Murray and D. H. Van Winkle, Phys. Rev. Lett. **58**, 1200 (1987).
[16] R. E. Kusner, J. A. Mann, J. Kerins, and A. J. Dahm, Phys. Rev. Lett. **73**, 3113 (1994).
[17] A. H. Marcus and S. A. Rice, Phys. Rev. Lett. **77**, 2577 (1996).
[18] P. Keim, G. Maret, and H. H. von Grünberg, Phys. Rev. E **75**, 031402 (2007).
[19] T. A. Weber and F. H. Stillinger, Phys. Rev. E **48**, 4351 (1993).
[20] E. A. Jagla, Phys. Rev. E **58**, 1478 (1998).
[21] A. M. Almudallal, S. V. Buldyrev, and I. Saika-Voivod, J. Chem. Phys. **137**, 034507 (2012).
[22] Y. Zhu, F. Wang, and H. Wu, J. Chem. Phys. **146**, 134703 (2017).
[23] H. Kleinert, Phys. Lett. A **89**, 294 (1982).
[24] H. Kleinert, Phys. Lett. A **130**, 443 (1988).

[25] Y. D. Fomin, E. Gaiduk, E. Tsiok, and V. Ryzhov, Mol. Phys. **116**, 3258 (2018).
[26] V. N. Ryzhov, E. E. Tareyeva, Y. D. Fomin, and E. N. Tsiok, Phys. Usp. **63**, 417 (2020).
[27] J. A. Anderson, J. Antonaglia, J. A. Millan, M. Engel, and S. C. Glotzer, Phys. Rev. X **7**, 021001 (2017).
[28] D. Abutbul and D. Podolsky, Phys. Rev. Lett. **128**, 255501 (2022).
[29] A. Skibinsky, S. V. Buldyrev, A. Scala, S. Havlin, and H. E. Stanley, Phys. Rev. E **60**, 2664 (1999).
[30] J. C. Armas-Pérez, J. Quintana-H, G. A. Chapela, E. Velasco, and G. Navascués, J. Chem. Phys. **140**, 064503 (2014).
[31] L. Q. Costa Campos, C. C. de Souza Silva, and S. W. S. Apolinario, Phys. Rev. E **86**, 051402 (2012).
[32] V. I. Kalikmanov, *Nucleation Theory*, Lecture Notes in Physics (Springer, Dordrecht, 2013).
[33] L. Q. Costa Campos, S. W. S. Apolinario, and H. Löwen, Phys. Rev. E **88**, 042313 (2013).
[34] W. Mickel, S. C. Kapfer, G. E. Schröder-Turk, and K. Mecke, J. Chem. Phys. **138**, 044501 (2013).
[35] R. M. Jungmann, P. C. N. Pereira, and S. W. S. Apolinario, J. Phys.: Condens. Matter **30**, 465402 (2018).
[36] K. Zahn and G. Maret, Phys. Rev. Lett. **85**, 3656 (2000).
[37] S. C. Kapfer and W. Krauth, Phys. Rev. Lett. **114**, 035702 (2015).
[38] A. Z. Patashinski, M. A. Ratner, R. Orlik, and A. C. Mitus, J. Phys. Chem. C **123**, 16787 (2019).